22nd Australasian Fluid Mechanics Conference AFMC2020
Brisbane, Australia, 7–10 December 2020
https://doi.org/10.14264/58eab30

High-Speed PIV Measurements of a Turbulent Boundary Layer at 80 kHz

P. Manovski[1,2], P. Gulotta[3], M. Giacobello[1], C.M. de Silva[4], N. Hutchins[2] and I. Marusic[2]

[1] Aerospace Division
Defence Science and Technology Group, Melbourne VIC 3207, Australia

[2] Department of Mechanical Engineering
University of Melbourne, VIC 3010, Australia

[3] Air Force Research Laboratory, United States Air Force, United States of America

[4] School of Mechanical and Manufacturing Engineering
University of New South Wales, NSW 2052, Australia

Abstract

This study reports the application of high-speed particle image velocimetry (PIV) to measure the mean and fluctuating velocity components in a turbulent boundary layer over a body of revolution. A narrow wall-normal strip of the flow field was captured using a synchronised high-speed laser and camera at a recording frequency of up to 80 kHz. The resulting high-speed PIV statistical quantities were shown to compare well with dual-pulse high-resolution PIV. The high-speed PIV streamwise velocity energy spectra were also found to compare well with hot-wire annemometry measurements at matched conditions.

Keywords
body of revolution; time-resolved; PIV; boundary layer.

Introduction

At the Defence Science and Technology (DST) Group, the PIV technique is routinely used to measure wake flow fields of subscale models. These databases are then employed to validate numerical simulations, see [1, 4], and references therein. In these studies, it was found that an important aspect in obtaining accurate flow fields from simulations is their ability to accurately model the near-wall flow characteristics, in particular at low angles of incidence where the viscous drag force dominates. Accurate measurement of the near-wall flow and turbulence levels is therefore of high importance. Of particular interest in the maritime and aeronautical domains is the flow over axisymmetric bodies of revolution. Slender axisymmetric bodies of revolution represent the simplest form of an aircraft fuselage or an underwater vehicle hull-form. This simplified test case serves as an excellent benchmark to assess measured near-wall flow quantities, before embarking on more complex geometries.

In Manovski et al. [4], a high resolution (6600 x 4400 px^2) camera with large focal length lens (400 mm) was used to conduct long-distance, high magnification PIV, which enabled near-wall measurements over a body of revolution. The mean and fluctuating velocity components of the turbulent boundary layer compared well with Pitot probe and hot-wire measurements. In that study, the boundary layer thickness and mean streamwise velocity were found to conform closely to a flat plate turbulent boundary layer in the parallel mid-body section of the geometry, where the flow is subjected to a near zero pressure gradient (ZPG). However, a comparison of the Reynolds stresses with direct numerical simulations (DNS) of a turbulent boundary layer (TBL) on a flat plate with ZPG indicated lower turbulence levels. This was partly attributed to the spatial averaging evident both in the hot-wire and PIV measurements. That investigation set the stage for future works using high-speed PIV experiments, which can provide additional insight, such as the spectral content. Accordingly, this study examines the boundary layer distribution over the same body of revolution with improved methods. In particular, the high-speed PIV method outlined by Willert [7, 8], is employed. Where a narrow strip of the flow field is illuminated by a high-speed laser and imaged by a high-speed camera to provide capture rates up to 80 kHz, allowing near time-resolved PIV velocity measurements. Here, the axial locations measured by Manovski et al. [4] have been repeated and the results between the different techniques are compared.

Test Facility and Model

The DST Low Speed Wind Tunnel (LSWT) is a closed-circuit tunnel that operates at atmospheric pressure. The test section is an irregular octagon, 2.74 m wide, 2.13 m high, and 6.56 m long. The free-stream streamwise turbulence intensity is less than 0.4%, and the transverse intensities are less than 0.7%.

The geometry used in this study is based on a concept design of a generic conventional diesel-electric submarine. The axisymmetric body of revolution or bare hull variant is tested here, and is without a casing and appendages. The model is shown in figure 1, and has length (L) of 2000 mm, and a diameter (D) of 273.66 mm. The model comprises a cylindrical centre-body with an ellipsoid nose and a streamlined tail section. The model was mounted on a twin aerofoil sliding rail support as shown in figure 1. A detailed description of the model geometry can be found in [4]. In the past decade, the bare hull and appended geometries have featured in numerous experimental and computational studies, see [1, 4] and references therein.

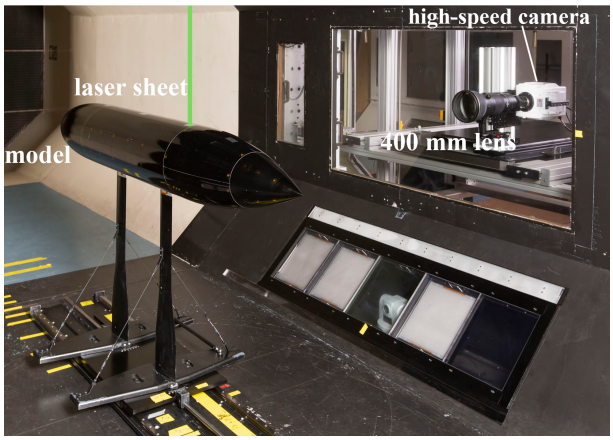

Figure 1. The body of revolution geometry and high-speed PIV experimental set-up, showing camera, lens, laser sheet and the model mounted with twin aerofoil sectioned supports.

The model was tested at zero incidence (yaw and pitch) with a tunnel airspeed of 28.8 m/s. The nominal Reynolds number based on the length of the model, $Re_L = 4.0 \times 10^6$. These flow conditions were chosen to match previous experimental tests. As described in [2, 4] a circumferential ring of trip dots was located on the nose at 5% of model length to enable laminar-to-turbulent transition of the surface flow. The trip dots are 0.29 mm tall, have a diameter of 1.27 mm, and are spaced 2.54 mm apart (centre-to-centre). The high-speed PIV measurements were conducted at axial stations, x/L = 0.25, 0.449, 0.65, 0.7, 0.8, 0.90, 0.97 and 1.02.

Test Technique – High-speed PIV

Two-dimensional (2D) PIV was undertaken with tracer particles (di-ethyl-hexyl-sabacate – DEHS) illuminated by an InnoLas Nanio Air 532-10-V-SP high-speed laser and imaged by a Phantom v2640 high-speed camera. The laser and camera synchronisation was provided by a LaVision PTU X. The displacement of particles in sub-regions (interrogation windows – IW) were determined by cross-correlation PIV software (LaVision DaVis 10.1). The laser light sheet was aligned with the streamwise direction with the camera orthogonal to the laser sheet therefore allowing the measurement of instantaneous streamwise (U) and wall-normal (W) velocity components.

The Innolas Nanio Air laser is an air cooled Nd:YVO_4 diode pumped solid-state laser with 532 nm wavelength and a typical operating repetition range of 20 – 80 kHz. The laser has a maximum pulse energy of approximately 550 μJ per pulse at 20 kHz, which is considerably smaller than ≈150 mJ pulse energies typical of dual cavity PIV lasers [4]. At 40 kHz the pulse energy reduces to ≈310 μJ, whereas at 80 kHz it is ≈140 μJ. The laser pulse width is 10 ns, 18 ns and 30 ns for 20 kHZ, 40 kHz, and 80 kHz, respectively, all of which are adequate to 'freeze' the motion of particles, for a typical PIV image magnification [5]. In order to maintain sufficient laser energy for PIV, the light sheet of the high-speed laser is limited to a narrow strip, approximately 6 mm × 55 mm, in the streamwise and wall-normal directions. This size strip was produced by a single cylindrical lens of -400 mm focal length. Additionally, two spherical lens of 1.5 m and 1.0 m focal length were placed in series to focus the laser sheet to a waist thickness of 0.6 mm (± 0.2 mm), as measured with burn paper.

Dual-pulse PIV lasers allow free adjustment of the time separation between laser pulses within the jitter rates of each laser cavity, thereby allowing the particle displacements to be optimised to the local flow velocity and PIV requirements. The InnoLas high-speed laser used in this study is a single cavity laser and was operated at a constant repetition frequency. Therefore, the time between pulses $\Delta t = 1/f$, where f is the repetition frequency. The maximum expected particle image displacement can be determined from the local free-stream airspeed, the laser repetition rate and the image magnification. For accurate PIV measurements, there are a number of factors, some of which are competing, that need to be taken into account when deciding on an appropriate Δt. A large Δt results in large particle displacements which can be desirable for a high dynamic velocity range and to reduce the statistical uncertainty of the measurement [5]. However, since the velocity measurement is temporally filtered, large displacements may cause bias errors due to flow acceleration or curved streamlines, as well as poor correlation due to particles leaving the IW or the light sheet plane [5]. Additionally, in the given configuration, the image width is cropped (144 px and 224 px) due to the narrow laser strip required to achieve high repetition rates. This further constrains the maximum displacement of particles. To ensure high particle detection probability, the in-plane displacements are limited to one-quarter of the linear dimension of the first IW [5]. To obtain several vectors across the width of the field-of-view, the initial size of IW should be 64 px – 96 px and therefore the maximum displacements of particles are limited to 16 – 24 px. This is consistent with Willert [7], who suggests limiting particle displacements between 10 – 20 px. Therefore in this study we restricted the maximum particle displacement to <20 px. It is often desirable in PIV measurements to maximise the spatial resolution in order to resolve flow structures. In the current study, high spatial resolution was desired to obtain near-wall measurements and to resolve the inner layer flow. A high spatial resolution is typically achieved by using a large focal length lens (as in [4]) to provide a high image magnification, but due to a fixed range of laser frequencies (and fixed Δt), increased magnification also increases particle displacements and imposes a requirement for higher particle densities. With all of this information at hand, working backwards from the maximum allowable particle displacement and the operating frequency range of the laser, a suitable range of image magnifications can be determined. Thus, for a free-stream of 28.8 m/s, a maximum displacement of 20 px and a frequency range of 20 kHz – 80 kHz, the suitable image magnification range is 14 px/mm to 56 px/mm. Ultimately, an image magnification of 24.62 px/mm was selected to allow for multiple capture rates and the effect of temporal filtering to be investigated at matched same spatial resolution. This magnification was achieved by using a large focal length lens, Nikon AF-S 400 mm G f2.8 lens with an actuated aperture control mechanism as described in [4].

The two capture rates investigated were 40 kHz and 80 kHz, with camera limitations requiring a cropped image width in the x-direction of 224 px and 144 px, respectively. The z-direction or wall-normal image resolution was kept constant at 1664 px. The 400 mm lens was operated at $f_\#$ (ratio of lens focal length to aperture diameter) of 2.8 to enable strong particle image signals. At this aperture setting some optical distortions and aberrations were evident around the outer perimeter of the full frame image (1952 px × 2048 px). However, these effects were negligible within the cropped image area (224 px × 1665 px). The camera on-board RAM (288 GB) allowed 500,000 and 800,000 samples to be collected over 12.5 s and 10 s, for 40 kHz and 80 kHz, respectively.

In order to compare the high-speed PIV with a reference PIV data-set, the measurement stations in [4] were repeated, this time with a higher resolution set-up. These measurements were achieved with a Nikon AF-S 300 mm f/4 lens fitted with a 3×teleconverter. This produced an effective focal length of 900 mm and for an observation distance of 1.5 m the spatial resolution was 121.2 px/mm. Apart from the lens, the experimental set-up was identical to that described in [4]. As in [4], elliptical Gaussian weighted IW with 4:1 aspect ratio were employed to maximise wall-normal spatial resolution while ensuring sufficient particle image counts. Due to the Gaussian weighting the elliptical IW can be considered to have an effective width of (2/3)×IW size (corresponding to ≈ 95% coverage). The experimental parameters for the new high resolution PIV and the high-speed PIV are summarised in table 1.

Results

The high-speed PIV measurements were conducted at eight axial stations along the model, however the focus of this paper will be at the axial station x/L = 0.449. At this location the boundary layer flow exhibits a near ZPG (≈ -0.4 Pa/m). Since the curvature parameter (defined as the ratio of the boundary layer thickness, δ_{99} = 13.39 mm, to the radius of curvature, r_m = 133.9 mm) is small (i.e. $\delta_{99}/r_m \ll O(1)$), the flow here should follow the canonical flat plate solution [4]. From [4], the

PIV camera	high-speed	high res.
frame rate, f (kHz)	40 / 80	0.0017
pulse separation, Δt (μs)	25 / 12.5	4
duration, T (s)	12.5 / 10.0	1,500
samples, N ($\times$1000)	500 / 800	3
TBL turn-overs, TU_∞/δ_{99}	2.3×10^4	4.0×10^6
sample interval, $u_\tau^2/(f\nu)$	2.4 / 1.2	5.7×10^4
measurement view, W (mm)	7.5 / 5	40
H (mm)	60 / 60	22
magnification, M (px/mm)	24.62	121.2
max displacement, Δ_{max}(px)	18 / 9	14
final elliptical IW, $W\times H$ (px^2)	24×6	36×9
effective IW width, (IW^+)	52	16
vector z res. (50% overlap), (z^+)	26	8

Table 1. Experimental parameters for the high-speed and high resolution PIV. The vector z-direction resolution is denoted – vector z res.

boundary layer characteristics at $x/L = 0.449$ are as follows, the estimated friction velocity, u_τ = 1.17 m/s, viscous length-scale, ν/u_τ = 0.012 mm (a '+' superscript indicates inner normalisation by u_τ/ν), the skin friction coefficient, $C_f = 0.00319$, and shape factor, $H = 1.40$. The corresponding momentum thickness Reynolds number, $Re_\theta = 3163$ and friction Reynolds number, $Re_\tau = 1087$. As in [4], the measured boundary layer data are compared with canonical flat plate DNS [6]. For the DNS, $C_f = 0.00312$, $H = 1.395$, $Re_\theta = 3270$ and $Re_\tau = 1040$, indicating only a small mismatch with our $x/L = 0.449$ data.

In figure 2, the results from [4] with wall-normal IW resolution of 22 wall-units (denoted '($IW^+ = 22$) PIV [4]' in the plots), are compared with the new high resolution set-up with resolution of 16 wall-units (denoted '($IW^+ = 16$) PIV') and the high-PIV cases (with $IW^+ = 52$). The boundary layer non-dimensional profiles are presented in figure 2 (a) and are scaled with the estimated friction velocity (u_τ = 1.17 m/s) as determined from the Clauser chart method, i.e. fitting the wall profile to the logarithmic law of the wall. The results from all of the techniques compare very well. The non-dimensional Reynolds stress profiles in the streamwise component, uu^+, and wall-normal component, ww^+ are compared in figure 2 (b). Similar to [4], an under-prediction of the turbulence levels is obtained compared to the DNS, and can be attributed to the spatial averaging due to the finite IW size and laser sheet thickness (ls_{th}^+ = 49 and 82 for the high-speed and high-resolution PIV, respectively). This was confirmed by using the method of [3], to filter the DNS to match the finite size of the PIV IW and laser sheet thickness, and is indicated by the DNS filtered to match PIV (IW^+, ls_{th}^+, IW^+) results in figure 2 (b). The good agreement between the PIV and the DNS filtered data validates the accuracy of the PIV data-sets. In figure 2 (c), ww^+ is plotted with linear scaling and shows the 40 kHz and 80 kHz data-sets. Due to the very high number of samples allowing better statistical convergence, the high-speed PIV profiles are smoother compared to the reference PIV results. The reference PIV data were acquired over much longer periods (1500 s) and therefore are more susceptible to variations in the tunnel velocity, which can bias the turbulent statistics. The standard deviation of the tunnel velocity for the high-resolution reference PIV was 0.028 m/s, whereas for both the high-speed PIV tests, the standard deviation was 0.013 m/s. To further investigate the effect of sample size, the 80 kHz results were recalculated with a reduced sample size of 6,000 (to match [4]). This was achieved by skipping 133 images between samples. The corresponding time separation is 1.67 ms (f = 600 Hz) or 3.6 TBL turn-overs between samples and as such, the samples may be considered statistically independent. The results for this case ('80 kHz – 133') are also indicated in figure 2 and show similar profiles to 80 kHz, with only a slight increase in the level of undulations.

Velocity spectra

The acquired velocity sample time is both sufficiently long and temporally well resolved to allow calculation of the power spectral density (PSD) of the fluctuating velocities (u and w), hereafter referred to as spectra. The spectra are presented in figure 3, at two wall-normal heights of $z^+ = 560$ ($0.5\delta_{99}$) and $z^+ = 100$ (which is in the log region). The spectra were calculated using the modified periodogram method of Welch with a Hanning window and 50% overlap. The inverse power law and a Kolmogorov -5/3 power law are also shown.

The high-speed PIV velocity spectra are compared with hot-wire data acquired from [4]. In that study, the hot-wire had a diameter of 5 μm and an active length of 1.17 mm ($l^+ = 95$). The anemometer voltages were sampled at 20 kHz for a period of 20 s, however the spectra were cut-off at 8.0 kHz due to the presence of spurious high frequency noise. Similar to the PIV results, an under-prediction in the turbulence levels compared to the DNS data was found with the hot-wire results and was due to its finite length [4]. As the hot-wire measures the resultant velocity magnitude (U_r) of the streamwise (U) and wall-normal (W) components, the same quantity (U_r) and its fluctuation (u_r) are calculated with the PIV data (as per [4]). Following [7], the cut-off frequency due to the finite sampling window size can be calculated. Here we take the effective IW size = 16 px = 0.65 mm and using the mean velocity of $\bar{u} \approx 25.47$ m/s at the measured height of z^+ = 560 and $\bar{u} \approx 19.09$ m/s at z^+ = 100. This results in an effective sample time of t_{IW} = IW/$\bar{u} \approx 26$ μs at z^+ = 560 and 34 μs at z^+ = 100. The inverse, $1/t_{IW}$ provides an estimate of the highest resolvable frequencies: 38.5 kHz at z^+ = 560 and 29.4 kHz at z^+ = 100. Taking the Nyquist cut-off from these values, the corresponding vertical lines are plotted in figure 3. The spectra for both 40 kHz and 80 kHz follow the hot-wire trend, with an initial linear decay until around 300 Hz, from which they follow the -5/3 power law reasonably well, until the cut-off frequency. The pre-multiplied spectra were calculated for the two wall heights, as shown in figure 3 (b) and (c). From the pre-multiplied spectra, in particular at z^+ = 100, it is apparent that the 80 kHz data follows the hot-wire and the power law more closely than the 40 kHz results, which 'kick up' >2 kHz. A similar trend was also obtained by sub-sampling every second image of the 80 kHz data-set to match the 40 kHz sampling rate. The higher temporal resolution and the smaller bias error (i.e. higher accuracy), afforded by the higher repetition rate, allows the higher frequency components to be better resolved. Due to the 55% reduction in pulse energy from 40 kHz to 80 kHz, the higher repetition rate results were expected to be noisier, however this effect was not pronounced. There is a small deviation in the 80 khz profile for f >3 kHz compared to the hot-wire, which warrants further investigation.

Concluding Remarks

This study reported the application of high-speed PIV to measure the mean, fluctuating velocity components and spectra in a turbulent boundary layer over a body of revolution. The two capture rates, of 40 kHz and 80 kHz, provided a comparison of the temporal filtering and allowed the limits of the method to be investigated. The high-speed PIV method was successfully validated against dual-pulse high resolution PIV and DNS. Both capture rates produced better converged turbulence profiles, as was evident by smoother profiles compared to dual-pulse PIV. It was found that the 80 kHz spectra compared better with the hot-wire measurements, owing to the higher temporal resolution and improved accuracy.

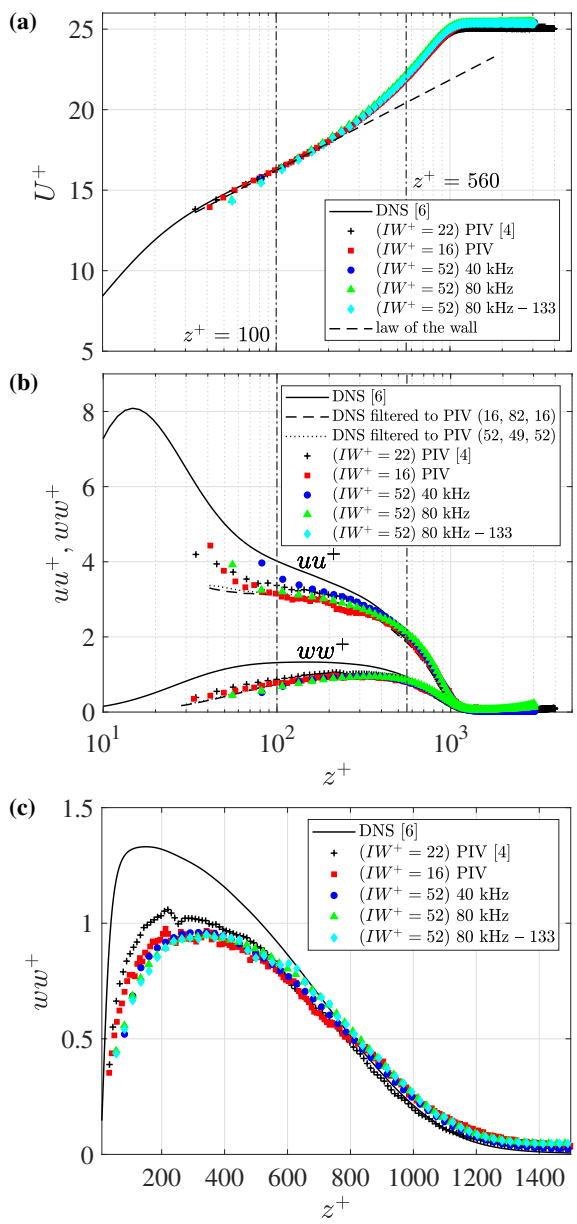

Figure 2. Boundary layer PIV results compared with DNS [6]. (a) Mean non-dimensional streamwise profiles. (b) Normalised Reynolds stress profiles in the streamwise component, uu^+, and wall-normal component, ww^+. (c) ww^+ plotted with a linear scale for z^+. The IW wall-normal resolution of each PIV method is indicated in wall-units (IW^+).

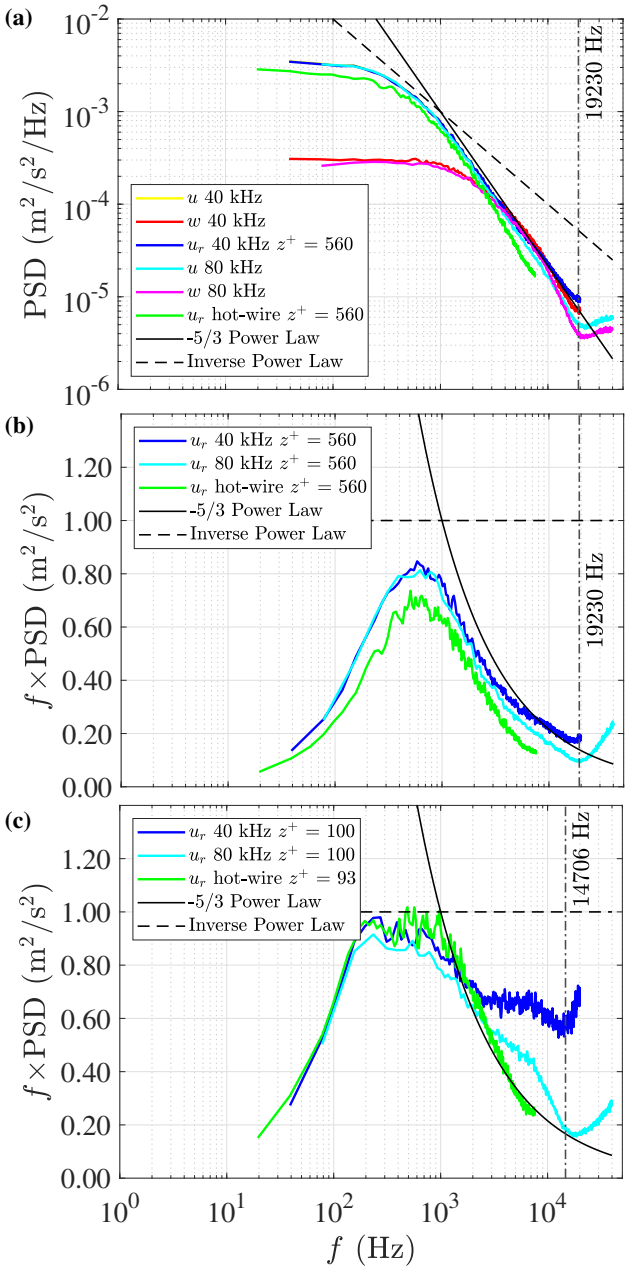

Figure 3. Spectra of velocity fluctuations, u, w and u_r for 40 kHz and 80 kHz high-speed PIV, as well as hot-wire from [4], (a) at $z^+ = 560$. Pre-multiplied spectra, (b) at $z^+ = 560$ and (c) at $z^+ = 100$.

References

[1] Fureby, C. et al, Experimental & numerical study of a conventional submarine at 10° yaw, *Ocean Engineering*, **116**, 2016, 1–20.

[2] Henbest, S. M. and Jones, M. B., Transition on a generic submarine model, Technical Report DST-Group-TR-3650, Defence Science and Technology (DST), Australia, 2020.

[3] Lee, J. H., Kevin, Monty, J. P. and Hutchins, N., Validating under-resolved turbulence intensities for PIV experiments in canonical wall-bounded turbulence, *Exp. in Fluids*, **57**, 2016, 129.

[4] Manovski, P., Jones, M. B., Henbest, S. M., Xue, Y., Giacobello, M. and de Silva, C., Boundary layer measurements over a body of revolution using long-distance PIV, *Int. Journal of Heat & Fluid Flow*, **83**, 2020, 108591.

[5] Scharnowski, S. and Kähler, C. J., Particle image velocimetry - classical operating rules from today's perspective, in *Optics and Lasers in Engineering*, 2020, number 106185.

[6] Schlatter, P. and Örlü, R., Assessment of direct numerical simulation data of turbulent boundary layers, *Journal of Fluid Mechanics*, **659**, 2010, 116–126.

[7] Willert, C. E., High-speed PIV for the efficient measurement of turbulence statistics, *Exp. in Fluids*, **56**, 2015, 17.

[8] Willert, C. E., "Profile-PIV" – More than just an optical hotwire: New potentials of particle image velocimetry in boundary layer research, in *18th International Symposium on Flow Visualization, Zurich, Switzerland*, 2018.